Electronic Supplementary Material (ESI) for Sustainable Energy & Fuels.
This journal is © The Royal Society of Chemistry 2024

Efficient hydrogen evolution from water over thin film photocathode composed of solid solutions with a composition gradient of ZnTe and CdTe

Lionel S. Veiga,[ab] Hiromu Kumagai,[a] Masakazu Sugiyama[ab] and Tsutomu Minegishi[ab]*

[a] Research Center for Advanced Science and Technology (RCAST), The University of Tokyo, 4-6-1, Komaba, Meguro-ku, Tokyo, JAPAN.

[b] Department of Advanced Interdisciplinary Studies (AIS), The University of Tokyo, 4-6-1, Komaba, Meguro-ku, Tokyo, JAPAN.

*Corresponding author: tmine@enesys.rcast.u-tokyo.ac.jp

S1 Effect of Cu thickness on the PEC properties of ITO/Cu/ZnTe/CdTe/CdS/Pt (RTA)

Figure S7A shows current-potential curves of CdTe based photocathodes prepared on ITO coated glass plates with different amounts of Cu additive prepared with sequential deposition of ZnTe and CdTe layers followed by rapid thermal annealing (RTA) process, chemical bath deposition (CBD) of CdS and vacuum evaporation of Pt (ITO/Cu/ZnTe/CdTe/CdS/Pt (RTA)). Thickness of ZnTe and CdTe layers were fixed at 3 mm. ITO/Cu/ZnTe/CdTe/CdS/Pt (RTA) with Cu thickness below 12 nm showed a confirmed cathodic photoresponse. However, their photocurrent values, especially at relatively high potential, were significantly changed. Cathodic photocurrent at low potential, 0 V_{RHE}, showed a trend of increasing with Cu layer thickness. In the case of ITO/Cu/ZnTe/CdTe/CdS/Pt (RTA) with Cu layer thicknesses of 0.5 and 1.0 nm showed 15.9 and 15.1 $mAcm^{-2}$ at 0 V_{RHE} while that with a Cu layer thickness of 12 nm showed 18.3 $mAcm^{-2}$ at 0 V_{RHE}. Structural characterisation results of SEM and XRD shown in Figures S8 and S9 reveal that the increase in Cu amount results in an increase in grain size, and Mott-Schottky plots also found an increase of acceptor concentration as shown in Figure S10. Increase of grain size and acceptor concentration are beneficial for decreasing series resistance, resulting in an increase of photocurrent especially at low potential region, around 0 V_{RHE}. On the other hand, too high an acceptor concentration is not beneficial for charge separation because of the decrease of depletion layer thickness. This decrease of depletion layer thickness was reflected in the decrease of onset potential (OP) and cathodic photocurrent at relatively high potential. ITO/Cu/ZnTe/CdTe/CdS/Pt (RTA) with Cu layer thicknesses of 0.5 and 1.0 nm showed 3.9 and 4.0 $mAcm^{-2}$ at 0.5 V_{RHE} while that with a Cu layer thickness of 12 nm showed 1.8 $mAcm^{-2}$ at 0.5 V_{RHE}. The OP also decreased from 0.7 to 0.66 V_{RHE} with increasing Cu layer thickness from 0.5-1.0 nm to 12 nm.

S2 Effect of ZnTe and CdTe thickness on the PEC properties of ITO/Cu/ZnTe/CdTe/CdS/Pt (RTA)

To investigate the impact of the ZnTe and CdTe layer thickness, ITO/Cu/ZnTe/CdTe/CdS/Pt (RTA) photocathodes with different ZnTe layer thickness were examined. Figure S11 shows current-potential curves of the ITO/Cu/ZnTe/CdTe/CdS/Pt (RTA) with different ZnTe layer thicknesses, with CdTe and Cu layer thicknesses fixed at 3 µm and 1 nm. The introduction of the ZnTe layer resulted in a noticeable enhancement of the photocurrent at 0 V_{RHE}, 0.5 V_{RHE}, and OP. However, 0.5 µm ZnTe on photocathodes increased the photocurrent at 0 V_{RHE} and OP from -8.0 to -14 $mAcm^{-2}$ and 0.65 V_{RHE}, respectively. For ZnTe layers thicker than the optimal 3 µm, the OP overcame 0.7 V_{RHE} slightly, and the photocurrent at lower potential remained similar. However, the photocurrent at around 0.5 V_{RHE} was clearly decreased from -4.0 to -3.1 $mAcm^{-2}$. Structural characterisation results for XRD and SEM-EDS are shown in Figures S12 and S13, respectively. The XRD pattern was not significantly affected by the ZnTe layer thickness while SEM-EDS reveal the structural differences: in the top-view SEM images, grain size increased with the ZnTe layer thickness, and, interestingly, the compositional ratio of Zn/(Cd+Zn) slightly increased with ZnTe layer thickness, indicating enhanced diffusion of Zn to the surface. To clarify the distribution of the compositional ratio, cross-sectional SEM-EDS analysis was performed as shown in Figure S14, and it was revealed that the ZnTe layer disappeared when the thickness was less than 3 mm, thus Zn diffusion to the surface direction was enhanced with an increase in ZnTe layer thickness until 3 mm. On the other hand, nothing but the size of grains found in top-view SEM image was enhanced by increasing the ZnTe layer thickness beyond 3 mm while series resistance should increase with thickness. To conclude, 3 mm is the optimal thickness of ZnTe from the viewpoint of forming a charge-selective back contact and composition gradient, to enhance charge separation and minimise series resistance.

Finally, the impact of CdTe layer thickness on ITO/Cu/ZnTe/CdTe/CdS/Pt (RTA) photocathodes were examined. Figure S15 shows current-potential curves of the ITO/Cu/ZnTe/CdTe/CdS/Pt (RTA) with different CdTe layer thicknesses, and ZnTe and Cu layer thickness fixed at 3 µm and 1 nm, respectively. The introduction of the CdTe layer resulted in a noticeable enhancement in the photocurrent at 0 V_{RHE}, 0.5 V_{RHE}, and OP. With a ZnTe thickness of 1.5 to 3 µm, the photocurrent at 0 V_{RHE}, 0.5 V_{RHE}, and OP increased from -8.0 to -15.1 $mAcm^{-2}$, -0.4 to -4.0 $mAcm^{-2}$, and from 0.63 to 0.7 V_{RHE}, respectively. Above a 3 µm CdTe thickness, the photocurrent remained stable. Plan-view SEM images of the samples illustrated the expected increase of the grain size with the augmentation of the CdTe layer thickness as presented in Figure S16. Complementary EDS-analysis of the surfaces revealed a significant variation in the composition ratio of Zn/(Cd+Zn). As is shown in Table S5, the increase in CdTe layer thickness imply a decrease in the Zn/(Cd+Zn), from 0.12 at 1.5 µm CdTe thickness to 0 at 4.5 µm CdTe thickness. These results strongly suggest that diffusion of Zn atoms across the CdTe layer is slower than the deposition ratio, leading to the formation of a solid solution of $Zn_xCd_{1-x}Te$ with a composition gradient and Cd-rich layer. The XRD patterns of samples with CdTe layers of 1.5, 2.4 and 3 µm also provide evidence of the formation of $Zn_xCd_{1-x}Te$. These patterns exhibit peaks corresponding to the diffraction planes of both CdTe and ZnTe, along with asymmetric peaks as shown in Figures S17A and S17B. Notably, the intensity of ZnTe peaks was less pronounced with the augmentation of the CdTe layer, disappearing completely on the sample with a CdTe layer thickness of 4.5 µm. Based on these structural characteristics, the increase of the photocurrent with the increase of CdTe layer thickness can be attributed to the formation of an efficient absorption layer, being the optimal thickness equal or above 3 µm.

Calculation of band diagram

The band diagram at the solid−liquid interface was calculated with the simulation software Afors-Het v2.5, utilizing the parameters listed in Table S1. The difference between the Fermi level (E_F) and the conduction band minimum for CdS, and between E_F and the valence band maximum for CdTe and ZnTe were assumed to both be 0.2 eV. The concentration of donors in the CdS layer and acceptors in the CdTe layer and ZnTe layer were assumed to both be 2 x 10^{17} according to the calculation from Mott-

Schottky plots. The VBM offset at the CdS/CdTe and CdTe/ZnTe interfaces were 0.85 and 0.27, respectivetly[1,2]. The flat-band potential for CdS, CdTe and ZnTe were set to be −0.26 V_{RHE}, 0.5 V_{RHE}, and 0.23 V_{RHE}.[2,3]

Table S1: Parameters used for the calculation of band diagrams.

Parameter	**CdS**	**CdTe**	**ZnTe**
Thickness (µm)	0.06	3	3
Dielectric constant	8.9 (4)	10.2 (4)	9.5(5)
Electron affinity (eV)	3.5	3.7	2.53
Bandgap (eV)	2.42 (4)	1.45 (4)	2.26(2)
Effective conduction band density (cm^{-3})	$7.9x10^{17}$ (6)	$3.4x10^{17}$ (6)	$3.1x10^{17}$ (6)
Effective valence band density (cm^{-3})	$1.8x10^{19}$ (6)	$1.2x10^{19}$ (6)	$1.5x10^{19}$ (6)
Electron mobility (cm^2/s)	100(7)	320(7)	340(8)
Effective hole density (cm^2/s)	25(7)	40(7)	100(8)
Acceptor density (cm^{-3})	0	$2x10^{17}$	$2x10^{17}$
Donator density (cm^{-3})	$2x10^{17}$	0	0

References

1 J. Fritsche, A. Thißen, A. Klein and W. Jaegermann, *Thin Solid Films*, 2001, **387**, 158–160.

2 J. Li, D. R. Diercks, T. R. Ohno, C. W. Warren, M. C. Lonergan, J. D. Beach and C. A. Wolden, *Sol. Energy Mater. Sol. Cells*, 2015, **133**, 208–215.

3 H. Kobayashi, N. Sato, M. Orita, Y. Kuang, H. Kaneko, T. Minegishi, T. Yamada and K. Domen, *Energy Environ. Sci.*, 2018, **11**, 3003–3009.

4 A. Morales-Acevedo, *Sol. Energy*, 2006, **80**, 675–681.

5 A. H. Reshak and S. Auluck, *Phys. B Condens. Matter*, 2007, **388**, 34–42.

6 O. Madelung, *Semiconductors: Data Handbook*, 2004.

7 Y. Chen, X. Tan, S. Peng, C. Xin, A. E. Delahoy, K. K. Chin and C. Zhang, *J. Electron. Mater.*, 2018, **47**, 1201–1207.

8 A. Kabalan and S. B. Sohid, *IEEE J. Electron Devices Soc.*, 2020, **8**, 701–710.

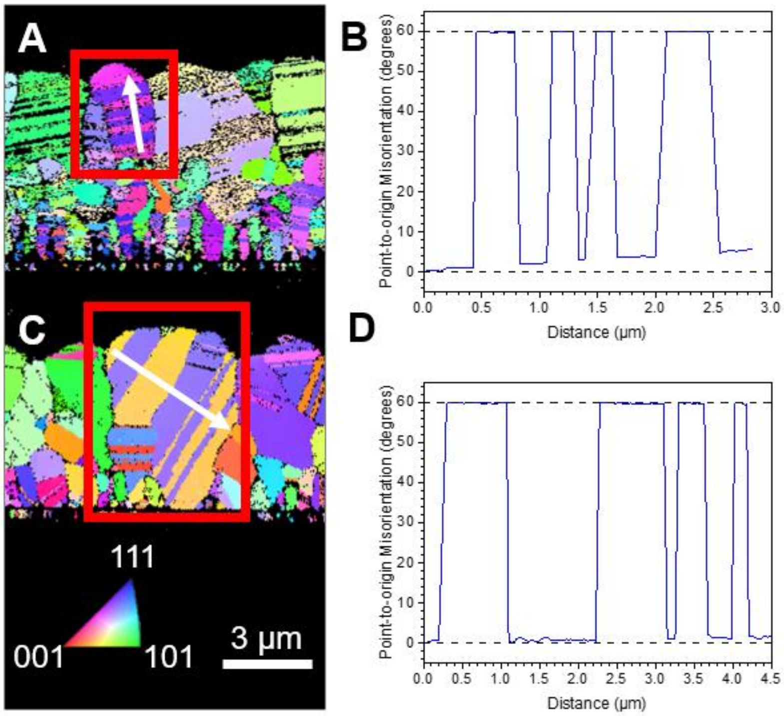

Figure S1: EBSD map for ITO/ZnTe/CdTe/CdS/Pt (A) and ITO/Cu/ZnTe/CdTe/CdS/Pt (C). The EBSD maps are normal-direction inverse pole figures (colour). (B) and (D) are the line analysis results of the point-to-origin misorientation for (A) and (C), respectively. The analysed areas in line analysis are indicated by arrows.

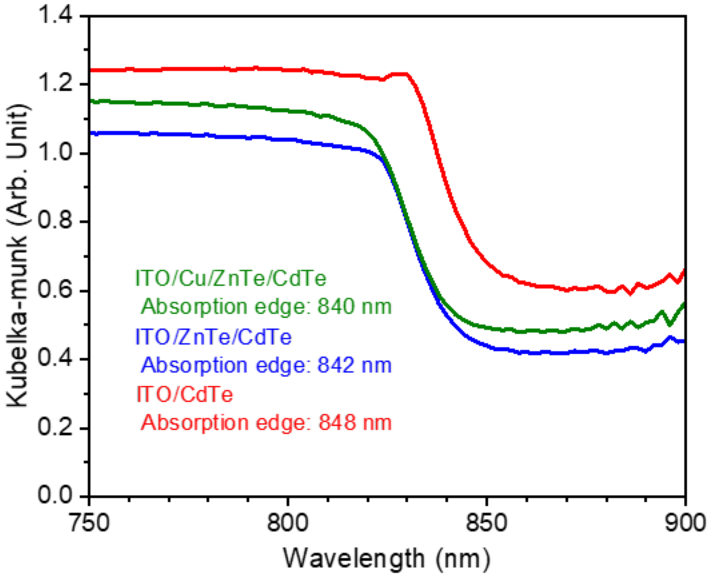

Figure S2: UV-vis DRS spectra obtained from ITO/CdTe, ITO/ZnTe/CdTe and ITO/Cu/ZnTe/CdTe.

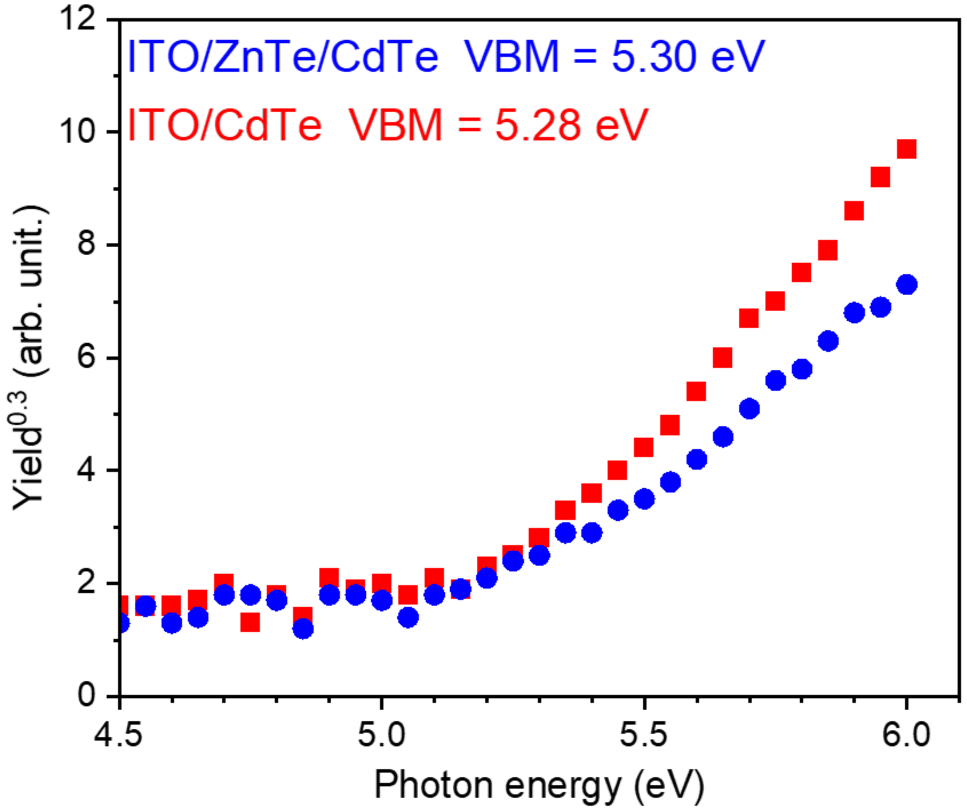

Figure S3: The PESA spectrum of ITO/CdTe and ITO/ZnTe/CdTe. The VBM potential was determined to be 5.28 and 5.30 eV, respectively.

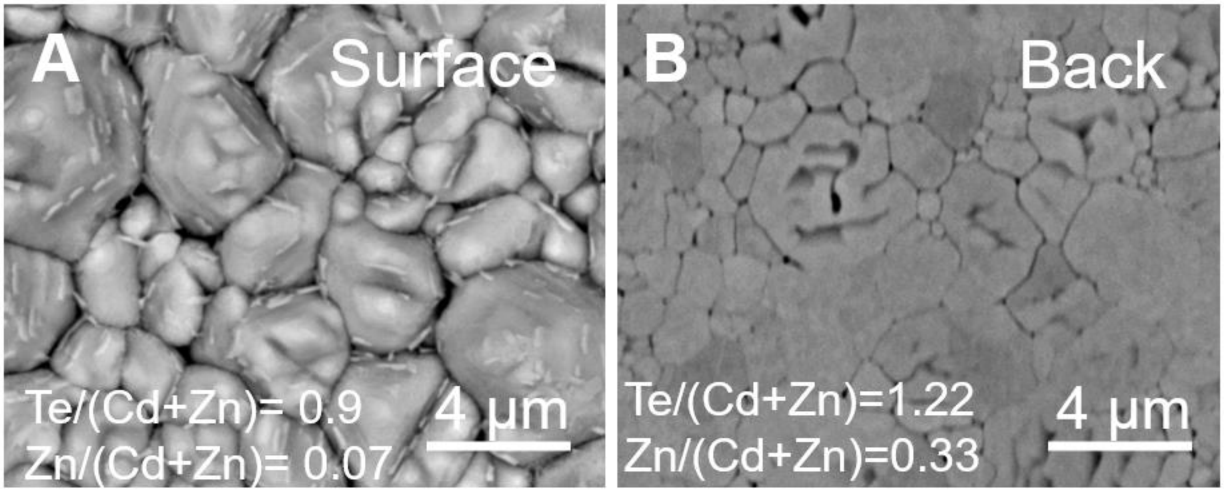

Figure S4: Front view (A) and back view (B) of ITO/ZnTe/CdTe after annealing treatment at 400°C for 15 minutes.

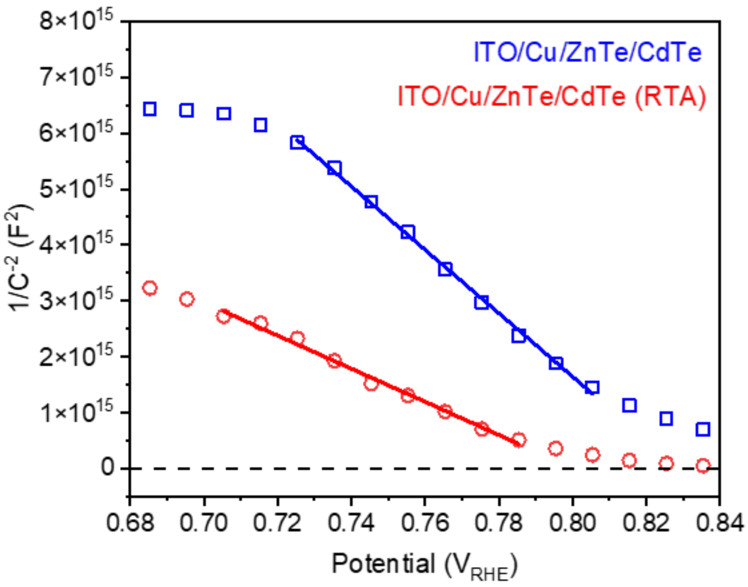

Figure S5: Mott-Schottky plots of ITO/Cu/ZnTe/CdTe (A), and ITO/Cu/ZnTe/CdTe (RTA) (B). A sinusoidal voltage perturbation with an amplitude of 10 mV and a frequency of 8000 Hz was superimposed on the potential applied by a potentiostat. An ideal RC series circuit was used as an equivalent circuit for analysis. A line plot was fitted to calculate the acceptor concentration.

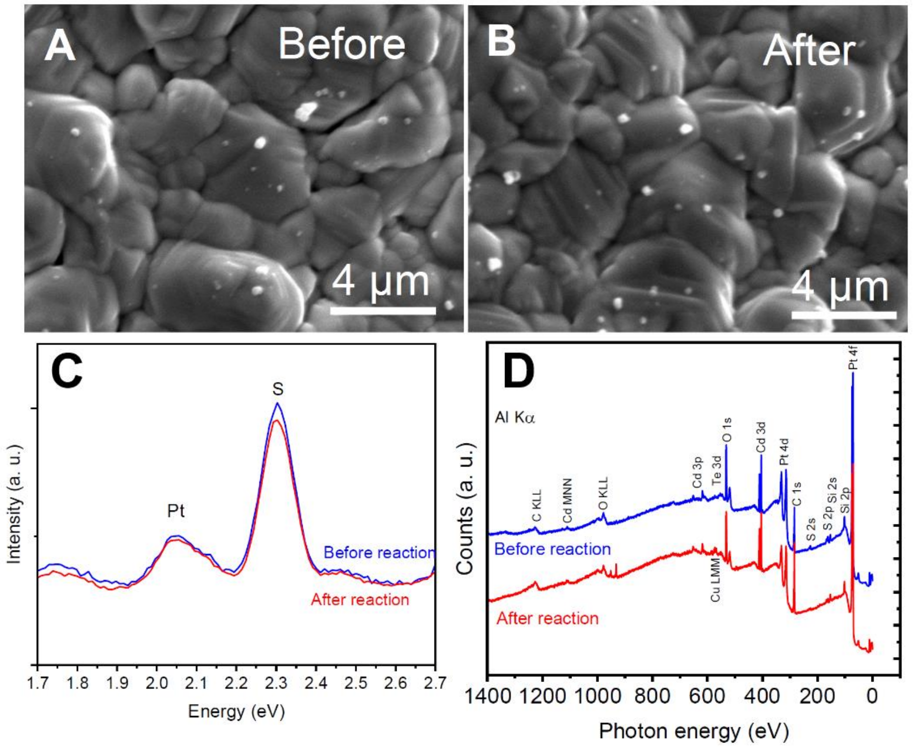

Figure S6: Plan-view of the ITO/Cu/ZnTe/CdTe/CdS/Pt +RTA, before (A) and after the reaction test (B), SEM-EDS spectra for before and after the reaction test (C), and XPS spectra for before and after the reaction test (D). Oxidation state of Pt for both before and after reaction test was metallic.

Table S2: Results of composition analysis from XPS spectra shown in Figure S6D.

	Before reaction	After reaction
Pt	12.2%	9.3%
Cd	3.1%	3.6%
S	2.9%	Not detected
Cu	Not detected	Trace (<0.1%)

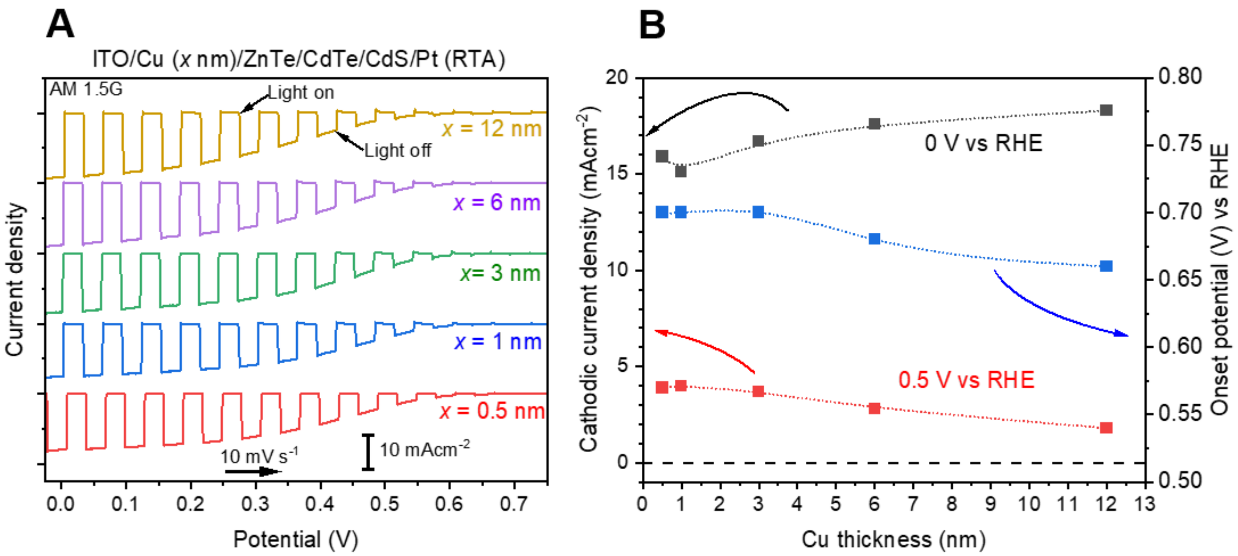

Figure S7: Current–potential curves (A) and summary (B) for photocathodes prepared from ITO/Cu/ZnTe/CdTe/CdS/Pt (RTA) with Cu addition of 0.5, 1, 3, 6, and 12 nm Cu layer. Measurements were done under chopped simulated sunlight in a 1 M aqueous KPi solution with pH adjusted to 6.5. The applied potential was swept at +10 mV s^{-1}.

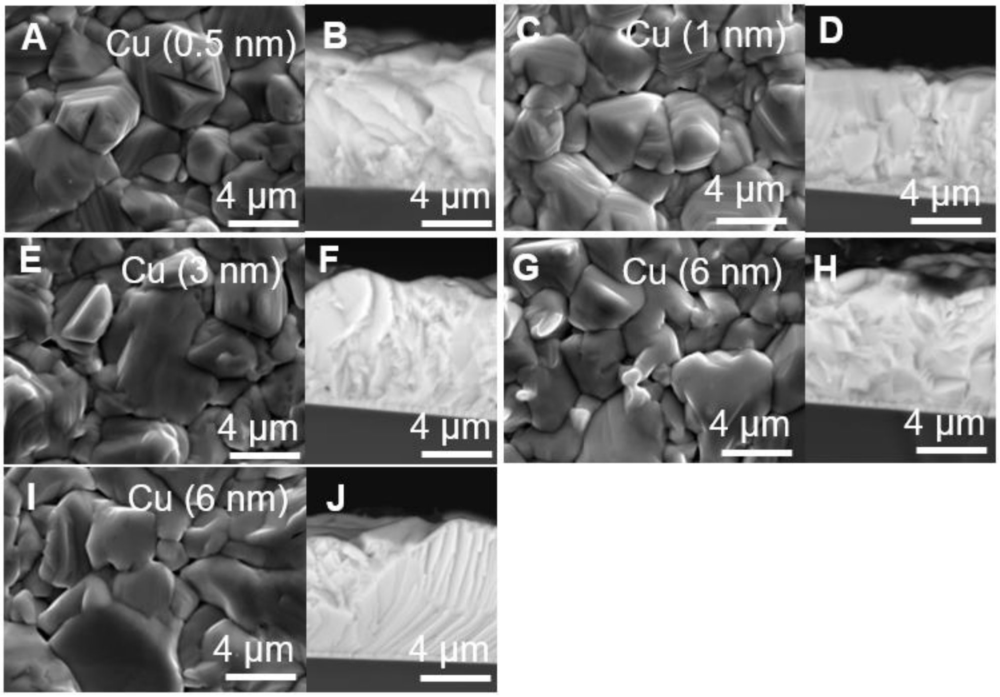

Figure S8: Plan-view (A, C, E, G, and I) and cross-sectional (B, D, F, H, and J) SEM images of ITO/Cu/ZnTe/CdTe with 3 µm CdTe layer, 3 µm ZnTe layer, and a Cu layer of 0.5, 1, 3, 6, and 12 nm.

Table S3: Results of composition analysis by SEM-EDS for ITO/Cu/ZnTe/CdTe/CdS/Pt (RTA) films prepared with Cu layer thickness of 0.5, 1, 3, 6 and 12 nm.

Cu thickness (nm)	Te/(Cd+Zn+Cu)	Zn/(Cd+Zn+Cu)	Cu/(Cd+Zn+Cu)
0.5	1.22	0	0
1	1.21	0.02	0
3	1.13	0.03	0
6	1.06	0.06	0.04
12	1.03	0.07	0.07

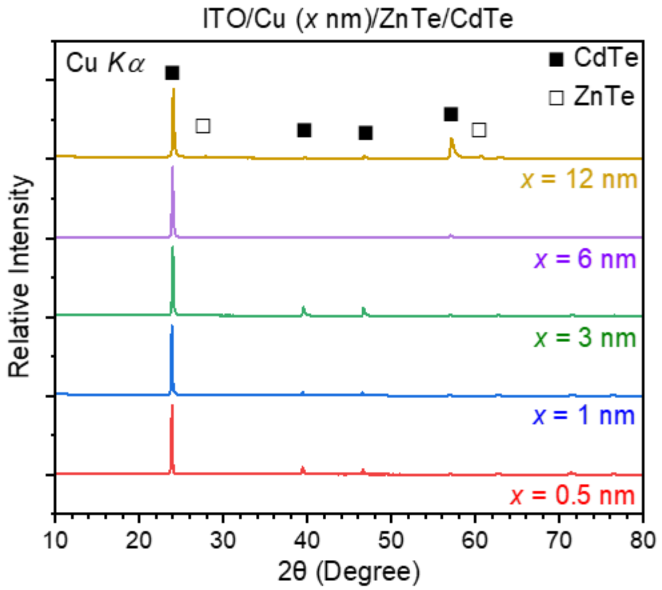

Figure S9: XRD patterns obtained from ITO/Cu/ZnTe/CdTe with 3 µm CdTe layer, 3 µm ZnTe layer and with a Cu layer thickness of 0.5, 1, 3, 6, and 12 nm.

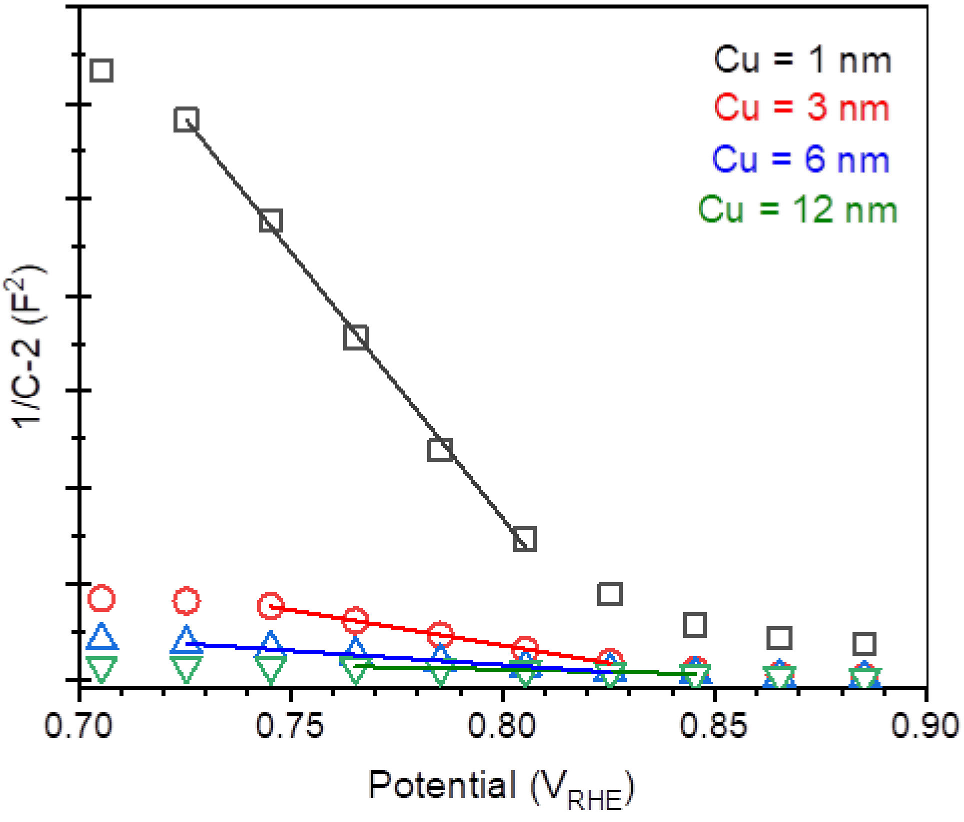

Figure S10: Mott-Schottky plots for ITO/Cu/ZnTe/CdTe samples with different Cu layer thickness. Acceptor concentration was calculated to be 3 x 10^{17}, 6 x 10^{18}, 7 x 10^{18}, 2 x 10^{19} cm^{-3} for the samples with Cu layer thickness of 1, 3, 6, and 12 nm, respectively.

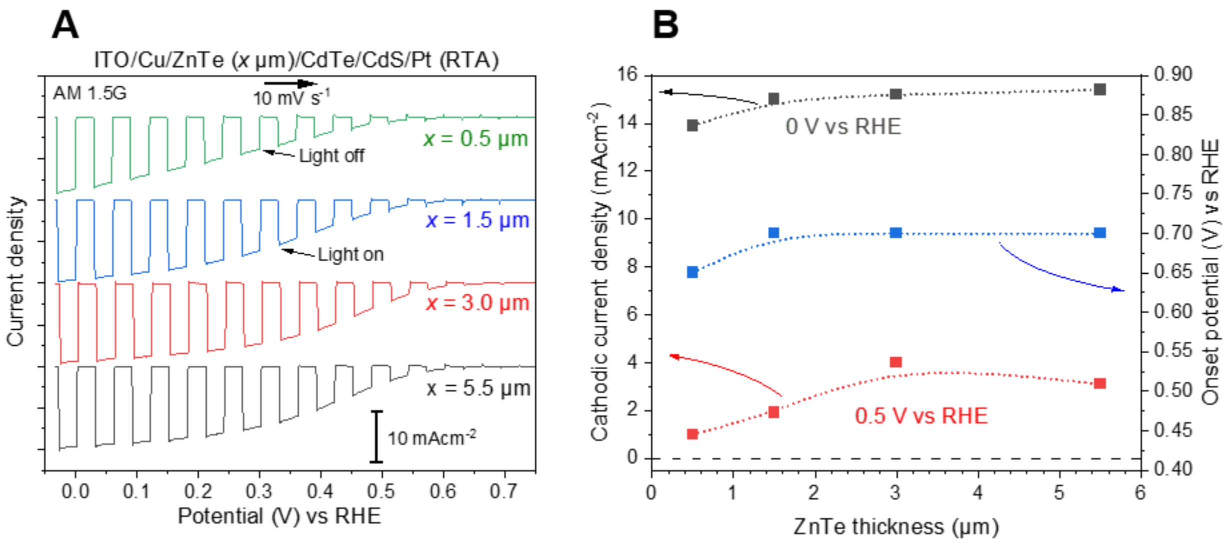

Figure S11: Current–potential curves (A) and summary (B) for photocathodes prepared from ITO/CdTe/CdS/Pt and ITO/Cu/ZnTe/CdTe/CdS/Pt (RTA) of samples with 1 nm Cu layer, 3 µm CdTe layer, and ZnTe layer of 0.5, 1.5, 3 and 5.5 µm. Measurements were done under chopped simulated sunlight in a 1 M aqueous KPi solution with pH adjusted to 6.5. The applied potential was swept at +10 mV s^{-1}.

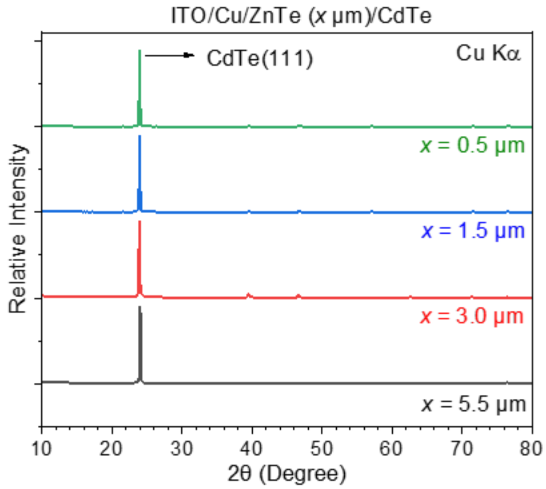

Figure S12: XRD patterns obtained from ITO/CdTe, and ITO/Cu/ZnTe/CdTe with 1 nm Cu layer, 3 µm CdTe layer, and ZnTe layer of 0.5, 1.5, 3 and 5.5 µm.

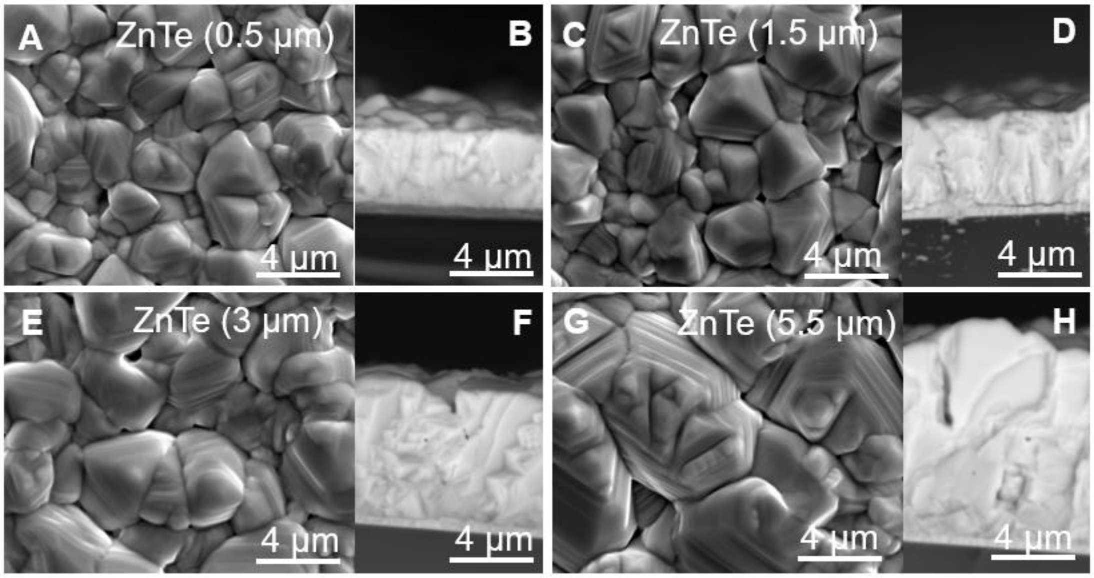

Figure S13: Plan-view (A, C, E, and G) and cross-sectional (B, D, F, and H) SEM images of ITO/Cu/ZnTe/CdTe with 1 nm Cu layer, 3 µm CdTe layer, and ZnTe layer of 0.5, 1.5, 3 and 5.5 µm.

Table S4: Results of composition analysis by SEM-EDS for ITO/Cu/ZnTe/CdTe/CdS/Pt (RTA) films prepared with ZnTe layer thickness of 0.5, 1.5, 3, 5.5 µm.

ZnTe thickness (µm)	Te/(Cd+Zn)	Zn/(Cd+Zn)
0.5	1.25	0
1.5	1.28	0.01
3	1.22	0.02
5.5	1.24	0

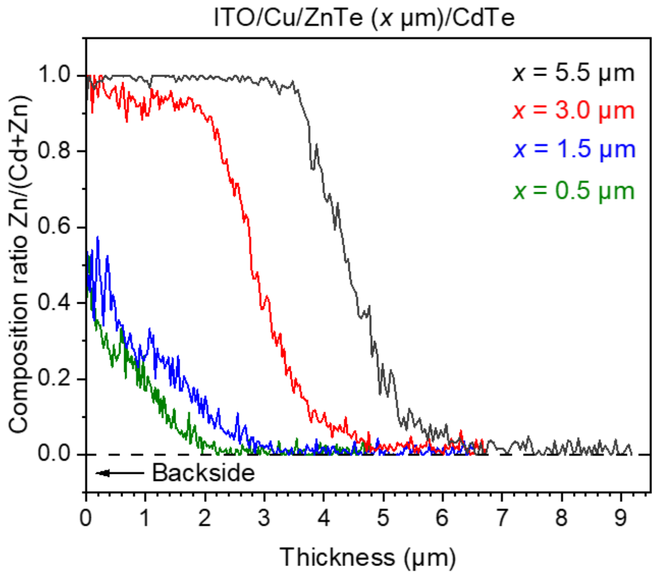

Figure S14: Composotion ratio Zn/(Zn+Cd) based on the SEM-EDS line analysis results from the cross-sectional SEM image of ITO/Cu/ZnTe/CdTe with ZnTe layer thickness of 0.5, 1.5, 3.0, and 5.5 μm.

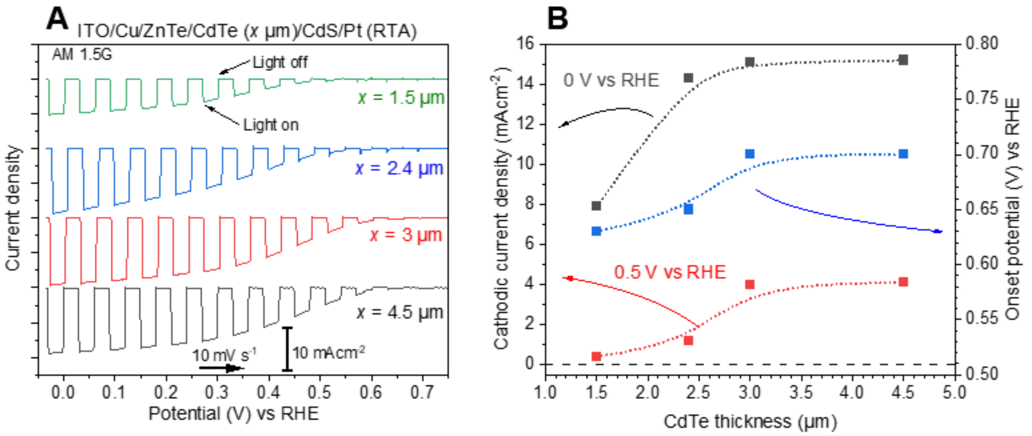

Figure S15: Current–potential curves (A) and summary (B) for photocathodes prepared from ITO/Cu/ZnTe/CdTe/CdS/Pt (RTA) of samples with 1 nm Cu layer, 3 μm ZnTe layer, and CdTe layer of 1.5, 2.4, 3 and 4.5 μm. Measurements were done under chopped simulated sunlight in a 1 M aqueous KPi solution with pH adjusted to 6.5. The applied potential was swept at +10 mV s^{-1}.

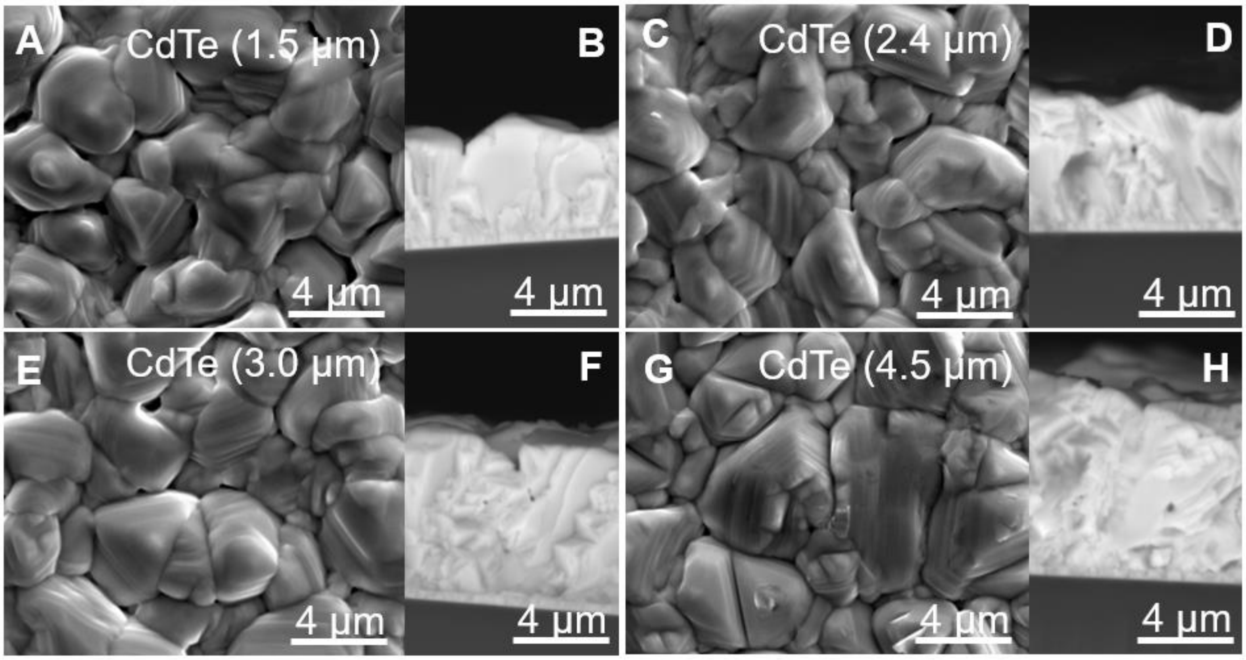

Figure S16: Plan-view (A, C, E, and G) and cross-sectional (B, D, F, and H) SEM images of ITO/Cu/ZnTe/CdTe with 1 nm Cu layer, 3 µm ZnTe layer, and CdTe layer thickness of 1.5, 2.4, 3 and 4.5 µm .

Table S5: Results of composition analysis by SEM-EDS for ITO/Cu/ZnTe/CdTe/CdS/Pt (RTA) films prepared with CdTe layer thickness of 1.5, 2.4, 3, 4.5 μm.

CdTe thickness (μm)	Te/(Cd+Zn)	Zn/(Cd+Zn)
1.5	1.25	0.12
2.4	1.27	0.04
3	1.22	0.02
4.5	1.24	0.00

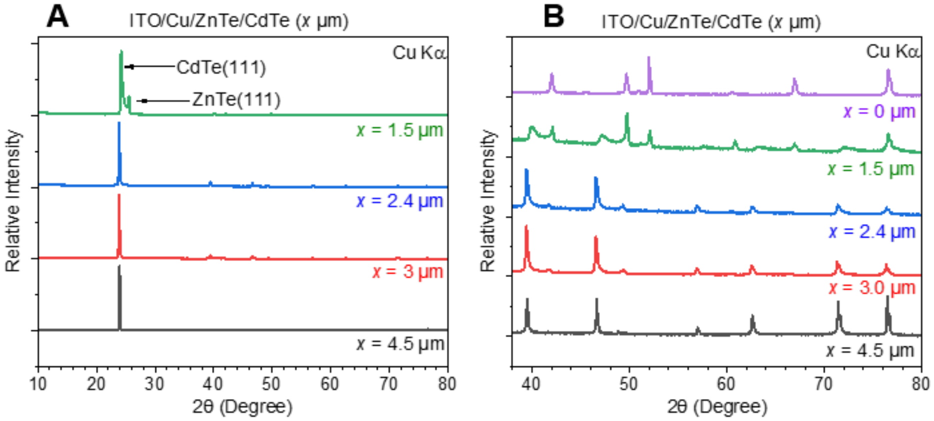

Figure S17: XRD patterns obtained from ITO/Cu/ZnTe/CdTe with 1 nm Cu layer, 3 μm ZnTe layer, and CdTe layer of 1.5, 2.4, 3 and 4.5 μm.

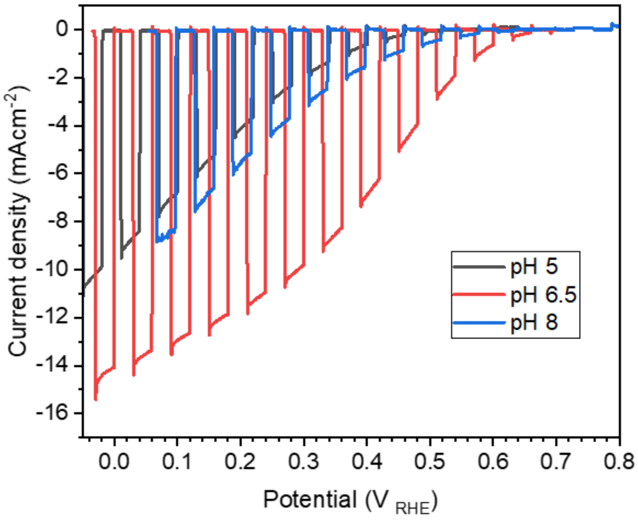

Figure S18: Current-potential curves for ITO/Cu/ZnTe/CdTe/CdS/Pt (RTA) under simulated light. 1 M aqueous KPi solution with pH values adjusted to be 5, 6.7, and 8.

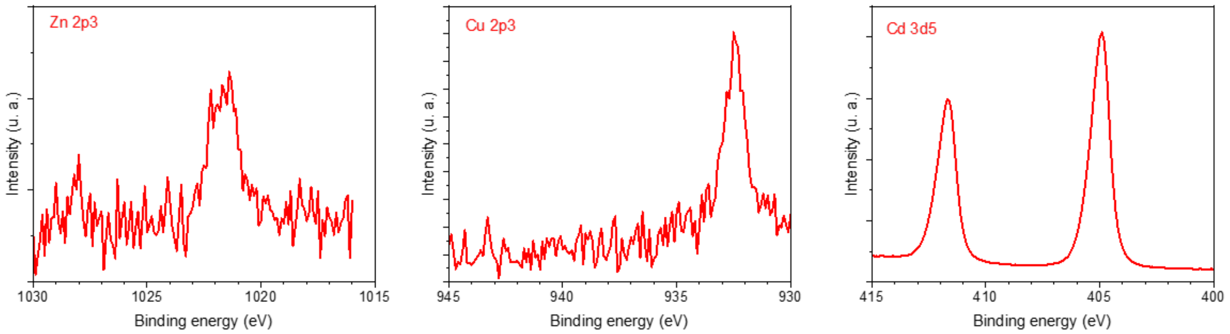

Figure S19: XPS spectrum for ITO/Cu/ZnTe/CdTe (RTA) focused on: (A) Zn, (B) Cd, and (C) Cd.